Metals and Materials International (2021) 27:2046–2058
https://doi.org/10.1007/s12540-020-00706-9

Fusion Weldabilities of Advanced High Manganese Steels: A Review

Gitae Park[1] · Seonghoon Jeong[1] · Changhee Lee[1]

Received: 23 January 2020 / Accepted: 17 March 2020 / Published online: 17 April 2020

Abstract
A large amount of manganese has been added to next-generation advanced high strength steels for automotive applications. The increased manganese content changes the microstructural and mechanical characteristics by varying both the stacking fault energy and the austenite stability, but it is known to deteriorate weldability. The current review provides a general strategy to address several problems in fusion welds of advanced high manganese steels from the viewpoint of microstructural transitions, plasticity mechanism, and mechanical properties based on the welding metallurgy. The importance of research on the weldabilities of advanced Mn steels was highlighted. Among the representative types of advanced manganese steels, this review focuses on high Mn twinning-induced plasticity steel, high Mn austenitic lightweight steel, and medium Mn transformation-induced plasticity steel. Specifically, this review suggests fundamental concepts for designing each steel with improved weld characteristics by presenting many research results on the correlations between the microstructure and mechanical properties of welds and heat-affected zones for these three different steel groups.

Keywords High manganese steel · Advanced high strength steel · Fusion welding · Microstructure · Phase transformation

1 Introduction

In recent years, there has been a significant increase in the demand for high-performance and eco-friendly materials in the global automotive industry to achieve better crush safety with increased fuel efficiency. Global auto manufacturers should meet the targets enacted under the Corporate Average Fuel Economy (CAFE) standards that forces substantial changes in automobiles to reach the target fuel economy and pollutant reductions [1–3]. The target conditions will continue to increase, as shown in Fig. 1, and hence automakers have demanded a high-performance material for weight reduction. Since there are substantial amounts of steels currently used in vehicles, automotive steel sheets have been developed to have better mechanical properties with lower density. Along with these developments, advanced high-strength steel (AHSS) has been attracting enormous attention as a high-performance automotive material [4].

Figure 2 is a representative diagram showing the mechanical characteristics of various automotive steel sheets at a glance [5, 6]. The first generation AHSS is a steel material with tensile absorbed energy of about 20,000 MPa %, and it was developed to replace conventional mild and high-strength steels after the oil crisis in the 1970s. Dual-phase (DP) and transformation-induced plasticity (TRIP) steels belong to this category [7, 8]. Until recently, GPa-grade tensile strength steels were obtained using a high fraction of martensite in their microstructures, but there is a limit to increasing the tensile absorbed energy because the strength and ductility are inversely proportion to each other due to the complex microstructures in the hard and soft phases in the steel [9]. Second generation AHSSs are high Mn twinning-induced plasticity (TWIP) steels possessing outstanding strengths of over 700 MPa and a remarkable ductility of higher than 50% [10]. The excellent elongation is based on a fully austenitic matrix and the dynamic Hall–Petch effect caused by twinning during deformation, which together result in a higher absorbed tensile energy. However, steel has disadvantages such as deteriorated weldability and high cost due to the substantial amount of alloying elements [11]. The third generation AHSS has a relatively lower tensile absorbed energy than the high Mn TWIP steels but are used to reduce vehicles weight or alloying elements. High Mn lightweight and medium Mn transformation-induced plasticity (TRIP) steels have been developed based on this concept.

✉ Changhee Lee
chlee@hanyang.ac.kr

[1] Division of Materials Science and Engineering, Hanyang University, Seoul 04763, Republic of Korea

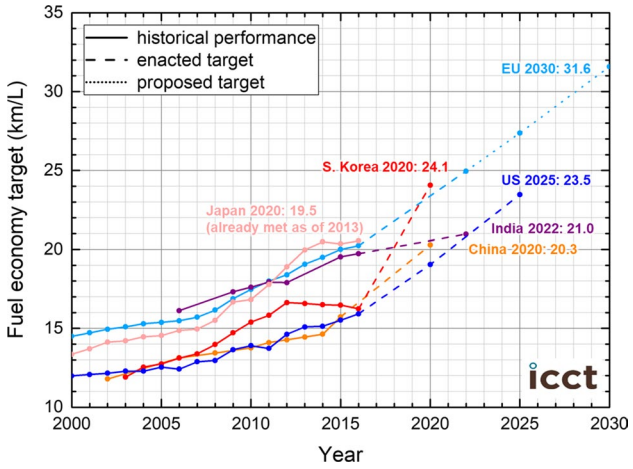

Fig. 1 Changes in historical performance and future targets for passenger automotive fuel economy in each country to comply with the Corporate Average Fuel Economy (CAFE) standard introduced in an effort to improve transportation efficiency and reduce the associated environmental emissions [1–3]

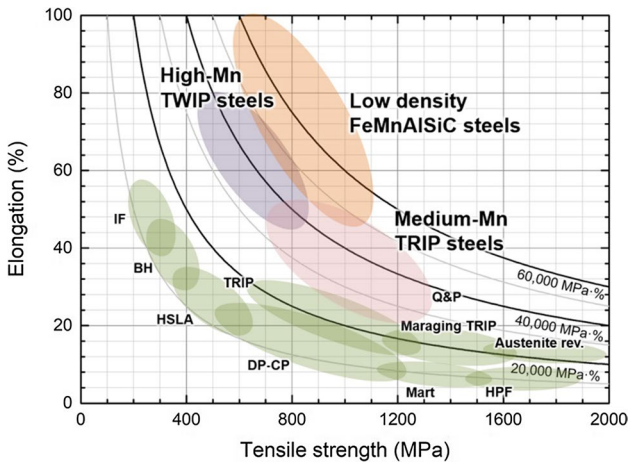

Fig. 2 Schematic diagram showing the relationship between elongation and tensile strength for automotive steels, which is commonly called a 'banana curve,' with emphasis placed on the three steel groups to be introduced in this review (redrawn from [5])

Degraded weldability has also been reported in several studies [12, 13], but more studies on the cause and solution are needed.

Welding is the most essential joining method for steel sheets in the vehicle manufacturing process. There are several welding methods used in vehicle manufacturing, including arc, resistance spot and laser welding [9, 14–16]. Regardless of the welding method, the welding process must lead to the formation of thermomechanically deformed regions during melting and solidification of the steel sheets. Most of the welds, including the fusion zone (FZ) and heat-affected zone (HAZ), exhibit deteriorated mechanical properties compared to the base metal (BM) [9]. This implies that the well-controlled microstructure, which is composed of retained austenite or a fully austenitic matrix at room temperature, can be destroyed and eventually become a different microstructure that degrades the mechanical properties. Therefore, there is a need to understand welding metallurgy. Specifically, we need to understand how higher contents of manganese affect changes in the microstructure and mechanical properties of the FZ and HAZ in advanced steel welds.

The current research largely focuses on representative advanced high manganese steels among various types of AHSSs, and we summarize the current research on their fusion weldabilities in this review. High Mn TWIP, high Mn austenitic lightweight and medium Mn TRIP steels will be discussed. Specifically, this review discusses what is detrimental in the weldability of each steel and what is needed to address the problem in the context of an overview of the metallurgical changes that occur during welding.

2 High Mn TWIP steels

In the steel industry, many researchers have historically focused on the role of manganese to reduce the high cost of raw materials by replacing nickel, which is a major alloying element but is not abundant in nature [17–19]. The purpose of manganese addition is both to strengthen the solid solution and to stabilize austenite at room temperature [10]. Along with this stabilization of austenite, various concepts of manganese-alloyed steels with unique deformation modes controlled by stacking fault energy (SFE) have been proposed. Among the advanced high manganese steels, the high Mn TWIP steel is a steel material utilizing a single-phase austenite having excellent formability due to its mechanical twinning. If a steel has a SFE within a range from 20 to 45 mJ m^{-2}, the formation of mechanical twins induces the creation of new crystal orientations in the austenitic matrix during deformation. Therefore, the chemical composition of the steel is varied to control the SFE (as shown in Fig. 3) in an effort to utilize the dynamic Hall–Petch effect that results in a high work hardening rate in steel [10]. In other words, the design of TWIP steel is based on adjusting the concentrations of the alloying elements to get the proper SFE value and to ensure a fully austenitic matrix.

Many different welding studies have been carried out for various applications. Weldability studies are roughly divided into groups according to the welding method: arc welding [11, 20], resistance spot welding [21], laser beam welding [22], friction stir welding [23], and electrical resistance welding [24, 25]. In many of these methods, the high alloying elements and the austenitic matrix of the TWIP steel substantially affect weldability [11, 17, 25], including special cases such as liquid metal embrittlement cracking

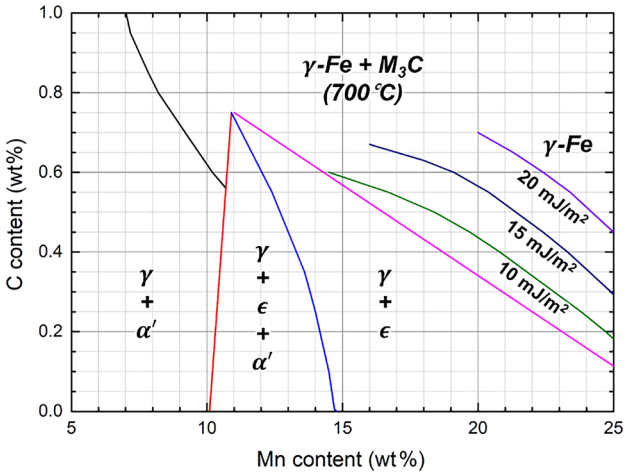

Fig. 3 Phase equilibrium after quenching from an annealing temperature of 700 °C and stacking fault energy according to the main alloying elements of high Mn TWIP steel present at room temperature (redrawn from [10])

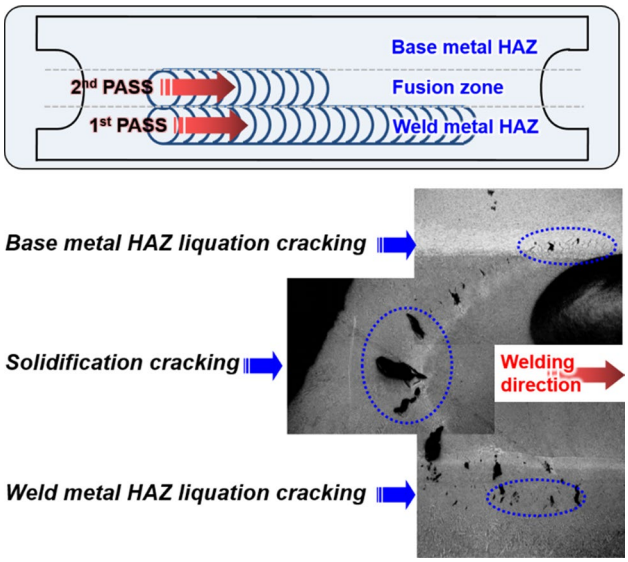

Fig. 4 Schematic diagram of double-pass longitudinal Varestraint test method and top-view macro image of the fractured specimen showing typical hot cracking after the test (redrawn from [27, 32])

by coating layers [21, 26]. The high content of alloying elements in the steel can change the mechanical properties of weldments by changing the solidification. This chapter focuses on what factors exist and how to control them in terms of solidification mode changes to improve the weldability of the TWIP steel.

2.1 Solidification cracking behavior of high Mn TWIP steel welds

In arc welds, solidification cracking is a critical weld defect that acts as a crack initiation site for structural failure. Unfortunately, high contents of alloying elements in many steels have been well-known to lower the solidification crack susceptibility [27, 28]. Many researchers have tried to understand and solve these problems, and several testing methods for evaluating the solidification cracking susceptibility were invented, such as Varestraint and Houldcroft tests [27]. Among them, the longitudinal Varestraint test is widely used as a test method to evaluate hot cracking susceptibility of steels including solidification, liquation and ductility dip cracking. The experiments have shown that a die block with a specific curvature results in strain under a specimen with a specific thickness when the arc weld passes, generating a partial crack due to stress during welding as shown in Fig. 4. The augmented strain is given by the following equation:

$$\text{Strain}\,(\%) = t/2R \times 100, \quad (1)$$

where the radius of the die block and the thickness are R and t, respectively. Hot cracking susceptibility is a characteristic of steel sheets, which are compared by the crack length generated in each steel material. For example, a steel with a higher total and maximum crack length (TCL and MCL) has a higher hot cracking susceptibility than the others, and hence its weldability is lower. Therefore, hot cracking behavior can be evaluated by comparing these crack lengths with various augmented strains.

Yoo et al. [11] investigated TCL and MCL of a representative high Mn TWIP steel (Fe–18Mn–0.6C) after double-pass longitudinal Varestraint tests. They suggested that the solidification cracking susceptibility of the steel lies in between those of STS304 and STS310S, as shown in Fig. 5. The main idea of their research is that the solidification mode of a weld affects several fundamental factors such as alloying element segregation into the dendritic boundaries and final solidification temperature. Weld metals of STS304 have an austenitic matrix with a vermicular type δ ferrite. That is, they solidified under the primary ferritic solidification mode (FA mode), so that their hot cracking susceptibility is lower than TWIP steel having a primary austenitic solidification mode (A mode).

It is well known that the amount of δ ferrite formed during solidification in a weld plays a decisive role in determining the hot cracking susceptibility of STS. Representative results of Lippold et al. [29] showed that STSs with ferrite numbers between 5 and 12 have better hot cracking susceptibility than those that are fully austenite. Similarly, Arata et al. [30] found that the austenitic STS welds containing 4–5% of δ ferrite were shown to be less susceptible than others containing more or less δ ferrite. The δ ferrite affects hot cracking susceptibility in five ways: grain refinement and impurity solubility, changes in interfacial energy that

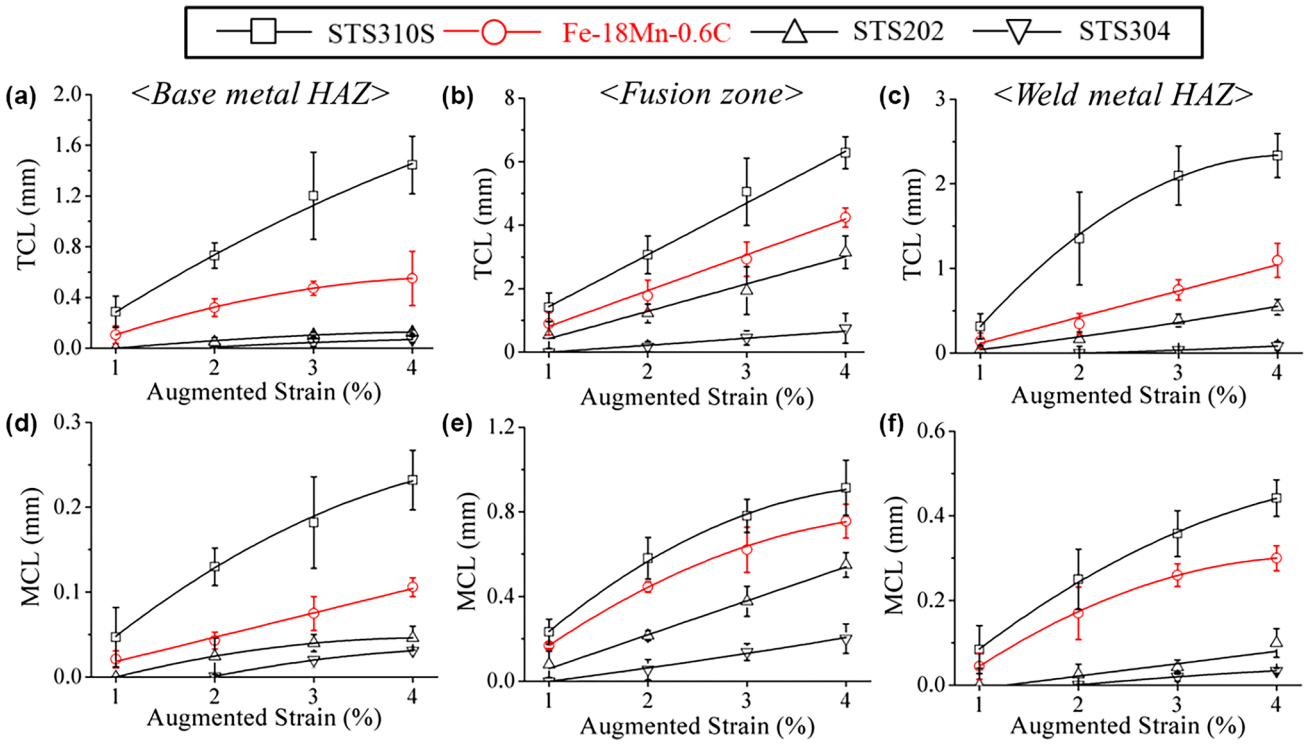

Fig. 5 Comparison of solidification cracking susceptibility of high Mn TWIP steel with conventional stainless steels. (**a**–**c**) Total and (**d**–**f**) maximum crack lengths (TCL and MCL) in the base metal, weld metal heat-affected zone (HAZ) and fusion zone were obtained from double-pass longitudinal Varestraint tests (Redrawn from [11])

reduce the wettability of eutectic films, volume contraction, changes in the solidification temperature range, and changes in ductility at high temperature [31]. Similar to the austenitic STS, the hot-cracking behavior of high Mn TWIP steels is closely related to the formation of δ ferrite. In the following section, the effect of each alloying element in TWIP steels on the hot cracking behavior will be discussed with respect to δ ferrite.

2.2 Effect of alloying elements on the solidification cracking susceptibility of high Mn TWIP steel welds

Like designing an STS weld, alloying elements in the high Mn TWIP steel need to be adjusted to obtain an appropriate amount of δ ferrite. An investigation of hot cracking susceptibility by adding aluminum [33] and chromium [34] to the basic TWIP steel composition of Fe–18Mn–0.6C [11] showed different behaviors depending on the resulting δ ferrite content, as shown in Fig. 6. These two elements are representative ferrite stabilizers and increase the delta ferrite content of TWIP steel welds. The base composition of TWIP steel has only small amounts of δ ferrite. As the alloying elements are added, increased amounts of δ ferrite play a very effective role in reducing hot cracking susceptibility.

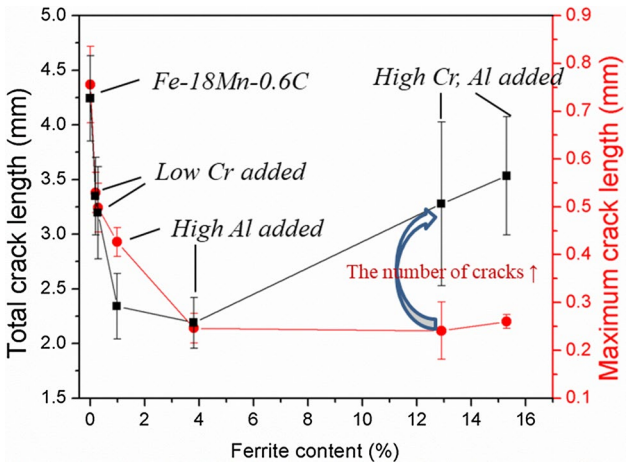

Fig. 6 Effect of δ ferrite content in weld metals of Fe–18Mn–0.6C TWIP steels with different chromium and aluminum concentrations (redrawn from [11, 20, 33, 34])

However, as the amount increases to values higher than approximately 10%, the hot cracking susceptibility increases again. The initial reduction effect due to the δ ferrite can be summarized in terms of the following mechanisms: (1) the formation of δ ferrite increases the inter-phase boundary region, which in turn may serve to reduce the amount

of segregation per area, (2) internal stress differences during welding due to the low volume expansion of δ ferrite, (3) the formation of δ ferrite may increase discontinuities when the liquid phase is present at the boundaries, and (4) grain refining effects. On the other hand, as the δ ferrite content increases, the influence of the characteristics of the ferrite increases. Since these properties are relatively lower than those of the austenite, the hot-cracking susceptibility increases.

In addition, silicon, the main alloying element of TWIP steel, increases the hot cracking susceptibility [20]. When solidification occurs during welding, the steel with silicon solidifies in the primary austenite mode, hence extensive segregation of silicon can occur. The segregated silicon shifts the eutectic carbon content to the lower side, thereby promoting eutectic behavior. The segregation also significantly affects the formation of secondary carbide formed after solidification. The formation of $(Fe, Mn)_3C$ eutectic carbide during solidification changes to a mixture of $(Fe,Mn)_{23}C_6$ and $(Fe,Mn)_5SiC$ due to the local partitioning of silicon and manganese in the steel. Eventually, three major alloying elements besides manganese were added to control the SFE of the steel, the fluidity of the molten pool, and the surface, but it is necessary to design the materials composition based on an understanding of the welding phenomenon related to the solidification mode.

In their excellent review paper, Mújica Roncery et al. [35] highlighted the need to control impurities in the TWIP steels such as phosphorous and sulfur. Although not published, our research group's experimental results [32] showed that increased phosphorous and sulfur content promoted crack formation, as shown in Fig. 7. That is, susceptibility to hot cracking can be reduced by elimination of impurities in the TWIP steels. This seems to be related to precipitates such as $(Fe,Mn)_3P$, but more research is needed. Recently, it has been reported that elements such as niobium [36], which form fine precipitates, can induce grain refinement in FZ and HAZ as well as in the BM. Therefore, to improve the weldability of TWIP steel, the formation of fine precipitates and segregation of impurities is required when designing an alloy an alloy design considering the solidification mode, formation of fine precipitates and segregation of impurities is required when designing an alloy, and the solidification mode must be considered.

3 High Mn austenitic lightweight steels

Lightweight steels were originally developed for replacing Fe–Cr-Ni stainless steels because of their appropriate corrosion resistance and price competitiveness [37–39]. Chem et al. [40] showed that using the plasma nitride process on austenitic lightweight steel results in remarkable hardening and superior corrosion resistance due to AlN formation. After several decades of work, however, scientists have focused more on a combination of density reduction and mechanical properties that meet both the occupant safety

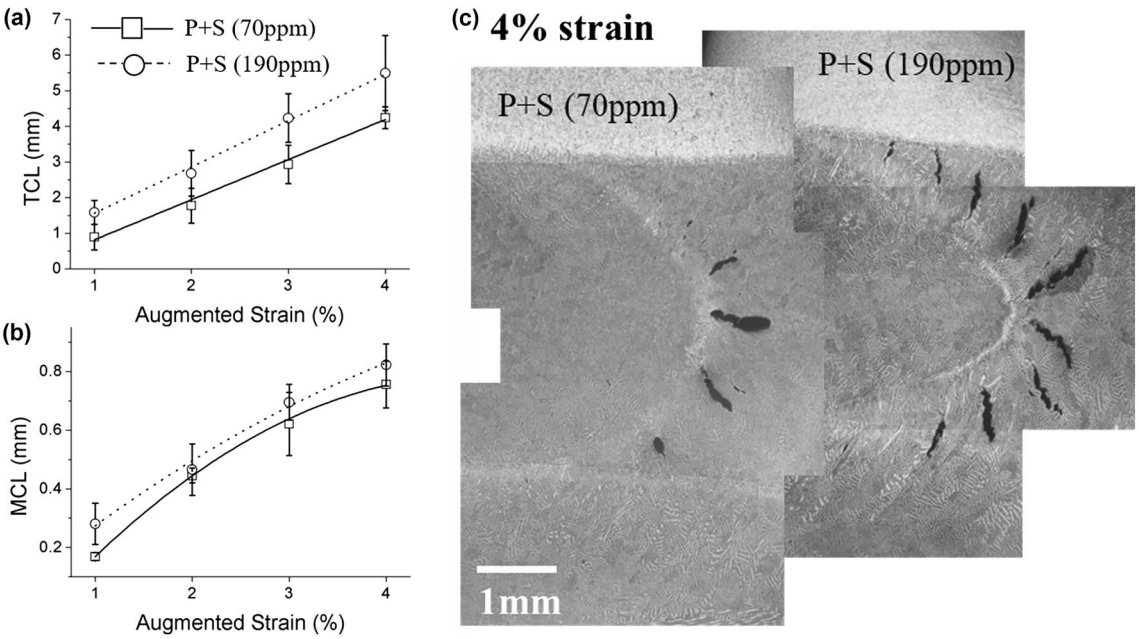

Fig. 7 Longitudinal Varestraint test results showing the effect of phosphorous and sulfur on the hot cracking susceptibility in Fe–18Mn–0.6C TWIP steel [32]: Comparison of (**a**) total, (**b**) maximum crack lengths, and (**c**) weld surface with the cracks

and environmental regulations for automotive applications [41–43].

As lightweight steels have attracted more attention, much alloy design work has been carried out based on thermodynamic calculations since the lightweight steels can be either austenite, ferrite, or duplex depending on the alloying content since Al is a ferrite stabilizer while Mn and C were austenite stabilizers. Thereafter, the austenitic lightweight steels, which was optimized with chemical compositions in the range of Fe–(15–30)Mn–(5–12)Al–(0.5–1.3)C, have been reported; these show outstanding performance without any deteriorative effect caused from the ferrite phase [44–49]. Several previous studies were conducted to understand density reduction effect., Mn, Al, and C are reported to have linear density reduction effects as the concentrations of the element increases. Mn has a lower molar density but larger atomic radius than Fe [50]. Al is also known for increasing stacking fault energy and effective weight reduction in austenitic lightweight steels [51, 52].

In addition to the density reduction effect, austenitic lightweight steel has also attracted great attention due to its unique plasticity phenomenon, which is mainly observed only in the austenitic lightweight steels. Scientists reported a unique dislocation behavior originating from a highly increased stacking fault energy (i.e. MBIP) that supported the strain-hardening increase and ductile characteristics [53]. Zhang et al. [54] observed the same phenomenon in several lightweight steels. Park et al. [55] calculated the relationship between stacking fault energy and deformation behavior transition between TRIP and TWIP and MBIP.

3.1 Base metal of austenitic lightweight steels

Various kinds of phase transitions can occur in the lightweight steels, and these have tremendous influence on both the microstructural and mechanical properties. Figure 8 shows a schematic illustration of the time temperature transformation diagram in Si added lightweight steel, which illustrates the phase transition behavior of DO3, B2, β-manganese, and κ-carbide. A DO3 (Fe_3Al) phase has been reported that precipitates on austenite grain boundaries or forms within the ferrite matrix via an ordering mechanism [56–58].

It has been reported that the DO3 phase shows increased strength and a ductility loss effect in the in Fe–Mn-Al-C alloys [59]. B2 is another phase that could be formed in lightweight steel as FeAl. Kim et al. [47] reported that the brittle B2 phase could provide a specific combination of strength and ductility. The formation of β-manganese, which appeared by excessive Mn addition and caused severe brittleness, was also investigated in terms of its effect on microstructure and mechanical properties. Lee et al. [60] confirmed that the addition of Al in the Fe–Mn-Al-C alloys

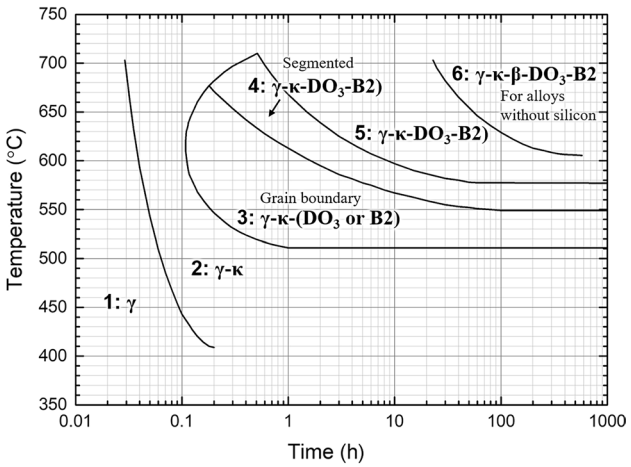

Fig. 8 Time-temperature-transformation diagram of Fe–28Mn–8.5Al–1C–1.25Si [58]

has an influence on the morphological transition and kinetics of the β-manganese formation. The κ-carbide phase, which has perovskite structures with $(Fe, Mn)_3Al$, is known to have the most important influence in the austenitic lightweight steels. Many analyses have been conducted to understand the effects of κ-carbide on the microstructure and mechanical properties, and it has been noted that nano-sized intragranular κ-carbide is coherent with a specific orientation relationship to the austenite matrix [48]. Various thermodynamic descriptions of κ-carbide were published such as first principles calculations or CALPHAD [61–63]. Bentley [64] investigated the isothermal age hardening process and showed that a temperature of 550 °C resulted in the maximum precipitation efficiency of κ-carbide with specific increases in mechanical properties. Moon et al. [65] summarized the microstructural evolution during isothermal age hardening in Fe–30Mn–9Al–0.9C alloys. Furthermore, the strengthening potential at appropriate temperatures in Fe–Mn-Al-C lightweight steel (which has a specific correlation with the behavior of κ-carbide content) has also been studied in detail [66, 67]. Figure 9 shows a comparison of the strengthening effect for various carbides in accordance with the precipitate fraction [68]. As shown in the figure, κ-carbide was confirmed to have precipitation strengthening potential comparable to micro-alloyed carbides such as NbC, VC, and TiC. Lee et al. [69] calculated that this strengthening effect in lightweight steels is induced by a κ-carbide shearing mechanism. Based on the literature, the precipitation behavior of κ-carbide is believed to have promising mechanical properties due to heat treatment.

Most phase transformations and ordering in lightweight steels are known to influence both the microstructure and mechanical properties, and this is mainly caused by Al addition. Moreover, it was revealed that an adequate level of

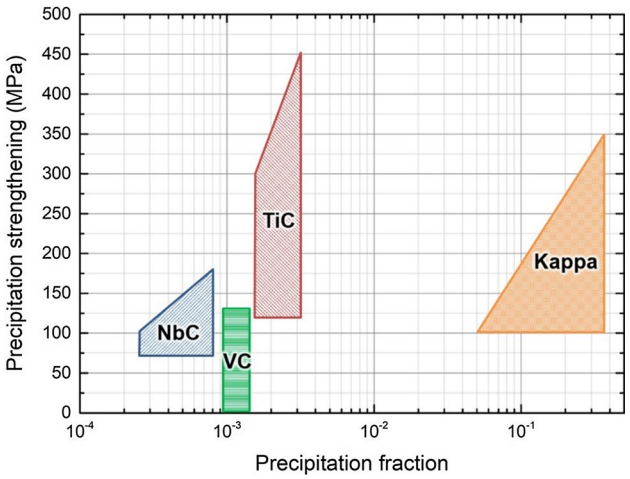

Fig. 9 Strengthening potential of the κ-carbide in lightweight steels comparted to NbC, VC, and TiC [68]

Al content increases the hardness and strength without a noticeable loss of ductility [70]. Other reports have been produced showing that C content has a remarkable influence on mechanical properties in many ways. Chang et al. [71] examined the tensile properties in Fe–29Mn–9Al alloys with different C contents, and they showed that increased carbon content results in great strength and elongation with a fully austenite phase. Using these alloying components as a basis, many kinds of alloying elements have been studied in lightweight steels and proved to have a specific influence on the Fe–Mn-Al-C alloy system. Kalashnikov et al. [72] reported the effect of various refractory elements on the mechanical properties such as V, Nb, W and Mo in the Fe–29Mn–9Al–0.9C alloy. Kim et al. [73] studied the effect of Si on the precipitation kinetics and interactions with dislocations. Moon et al. [74] investigated the effect of Mo addition at the atomic scale. The effect of Cr addition on the microstructure and mechanical properties has also been reported in the Fe–30Mn–10.5 Al–1.1 C alloy [75].

The potential usefulness of lightweight steels confirmed the importance of analyses and considerations for the welding process and the ultimate characteristics. Since lightweight steels can have rapid phase transitions as the temperature changes, other studies focused on weld metal and HAZ in lightweight steels have been conducted.

3.2 Weld metal characteristics in austenitic lightweight steels

It is well known that large amounts of alloying elements can reduce the weldability. For instance, there are potential problems due to the nature of manganese such as widening of the solidification temperature range or evaporation in the fusion zone [76]. In addition, studies on the weldability in austenitic lightweight steels using high fractions of various elements have been produced, and inferior fusion zone properties were observed in comparison to base steel.

Ku et al. [45] investigated Fe–28Mn–5Al–1C alloy with respect to microstructure and mechanical properties in EBW and LSW welding procedures. In the introduced alloy, tensile strength and ductility loss occurred with partial cleavage fracture during the tensile tests, regardless of the welding methods. Impact toughness degradation in weld metal was revealed due to a mixed microstructure with austenite, κ-carbide, and small amounts of ferrite. The microstructural transition in the Fe–30Mn–9Al–0.4C alloy as a weld metal revealed a rapid DO3 precipitation mechanism during GTAW [77]. The authors also mentioned ductility loss in the butt-jointed welded sample. An incompletely melted zone has been discovered at the interface of the fusion zone with phase transformation, which was explained in terms of thermal history [78].

To improve the weldability and fusion zone properties of lightweight steels, many investigations on welding with various experiments have been performed. Chou et al. [79–81] reported the hot cracking susceptibility of Fe–30Mn–(8–10)Al–(0.12–1.17)C lightweight steels. The authors said that four types of microstructural evolution: vermicular ferrite, lacy ferrite, acicular austenite growing from a ferrite matrix, and Widmanstatten austenite growing from austenite boundaries could be found in the weld metal in the experimental alloys. It was also reported that the Widmanstatten austenite and acicular austenite had a great hot cracking susceptibility. Furthermore, a strong relationship between carbon content and ferrite was confirmed, and the alloys with a proper fraction of ferrite exhibited beneficial influence on the hot cracking resistance.

Overall, the hot cracking show that lightweight steels have complex ductility behavior at elevated temperature and other factors also affect the properties. Figure 10 shows the representative hot-ductility behavior upon a cooling thermal cycle in the Fe–30Mn–9Al–0.9C alloy [82]. Grain boundary solidification in a partially melted zone, dynamic recrystallization (DRX) induced by plastic deformation, and the MBIP effect might have increased ductility in the lightweight steels. On the other hand, a drop in ductility occurred due to grain growth or DO3 precipitation during the cooling cycle. The formation of DO3 in the welding condition is of interest due to its unique effects. Lin et al. [83] investigated the phase transition mechanism from 550 to 600 °C in the Fe–26.6Mn–8.8Al–0.61C and confirmed that weld metal and base steel had different phase transition behavior due to the segregation of Al during the welding process. The weld metal had a phase transition sequence from DO3 to B2, and ferrite with a DO3 phase eventually transformed into the B2 phase in the base steel.

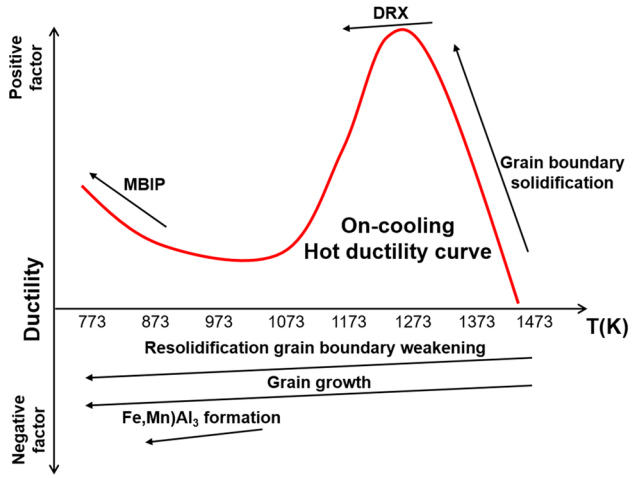

Fig. 10 Schematic illustration showing the effect of individual factors on hot ductility and the net-ductility curve on the cooling thermal cycle in Fe–30Mn–9Al–0.9C [82]

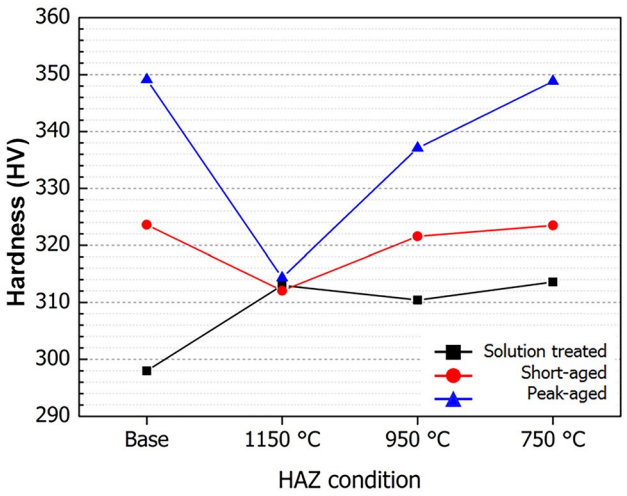

Fig. 11 Hardness profiles of HAZs with various peak temperatures and age-hardening conditions in the Fe–31.4Mn–11.4Al–0.9C [86]

3.3 HAZ properties in austenitic lightweight steels

Scientists agree on the need for analyses focused on the HAZ characteristics since the HAZ properties in austenitic lightweight steels are known to have significant effects. As a result, many studies on understanding the HAZ properties in Fe–Mn-Al-C alloys have been published.

Tjong et al. [84] reported the HAZ hardness transition behavior after the EBW process in the Fe–28Mn–6Al–1C alloy. The authors suggested that the increased hardness in the HAZ is related to the strain induced twinning mechanism, while decreased hardness and the creep rupture life of the fusion zone came from the parting of the dendrite phase. In later studies, the effect of κ-carbide has been confirmed in the HAZ mechanical properties. Jeong et al. [85] investigated the relationship between microstructure and mechanical properties in the Fe–30Mn–0.9C–xAl lightweight alloys, revealing the influence of κ-carbide precipitation in HAZs with various heat input conditions. The existence of intra-granular and inter-granular κ-carbide and their influence on the in HAZ properties were described in detail. As the content of Al increased, the precipitation of intra-granular κ-carbide in HAZs accelerated while maintaining the [011]γ//[011]κ crystallographic relationship. This coherent κ-carbide showed a direct relationship with tensile and hardness properties for all examined specimens. However, due to the formation of inter-granular κ-carbide, the cryogenic impact toughness of HAZ decreased dramatically in the alloys with higher Al content, despite the robust combination of strength and ductility. TEM analysis showed the presence of large inter-granular κ-carbide particles with an irregular shape in the HAZ that triggered brittle cleavage fracture.

The same author noted the deleterious effect of κ-carbide precipitates on mechanical characteristics in the Fe–31.4Mn–11.4Al–0.9C alloy [86]. Figure 11 shows the hardness transition behavior in HAZs for solution treated, short-aged (10 min at 550 °C), and peak-aged (100 min at 550 °C) cases. The peak temperatures for HAZs were 1150, 950, and 750 °C. The HAZ was hardened due to the rapid precipitation of κ-carbide in the solution treated state. On the other hand, HAZ softening also occurred during age-hardening because the κ-carbide in HAZ at high temperature was completely dissolved during the welding thermal cycle. Further, the inter-granular κ-carbide resulted in severe brittleness in the impact toughness test, and the author suggested not to put an excessive amount of Al in the Fe–Mn-Al-C alloy. The κ-carbide also had a significant impact on grain boundaries at elevated temperature. Kim et al. [87] confirmed that the precipitation of κ-carbide at high temperature causes local HAZ cracking with Varestraint tests. The experiments also confirmed that inter-granular cracking was induced by the relative weakness of the grain boundary and inter-granular κ-carbide formation at in situ at high temperature.

The effect of refractory elements was explored in the tensile properties of HAZs. Moon et al. [88] investigated the effect of V and Nb addition to the Fe–30Mn–9Al–0.9C alloy. The experimental results showed that the tensile properties could be enhanced by the addition of refractory elements with the grain refinement effect and precipitation hardening from the formation of VC, NbC, or (V, Nb)C. Those particles precipitated both in the matrix and grain boundaries.

4 Medium Mn TRIP steels

As a third-generation AHSS, medium Mn TRIP steels have been attracting attention for use in automotive application to improve the fuel efficiency of vehicles. This steel has been extensively investigated to replace conventional hot-stamping boron steels for automotive applications due to its relatively lower press forming temperature in addition to outstanding mechanical properties [6, 89]. Alloying elements in the steel are basically designed to make good use of the TRIP effect of the metastable austenite using the high content of manganese (3–10 wt%). Because a dual-phase matrix of ferrite and austenite is formed through intercritical annealing, many researchers have been focused on achieving improved mechanical properties by controlling intercritical annealing conditions [90, 91]. At this time, redistribution of manganese between the two phases is the key determining how to obtain stable austenite at room temperature. The accumulation of the manganese into the austenite lowers the SFE, resulting in a TRIP phenomenon that is essential for achieving excellent mechanical properties. However, the problem is that these well-controlled microstructures must be changed after welding and inevitably degrade the mechanical properties.

Like the other advanced high manganese steels, the weldability problem is based on phase transformation due to rapid thermo-mechanical cycling of the weld. Studies on the weldability of medium Mn TRIP steel have commonly pointed out that the decrease in the mechanical properties in weldment is related to the brittleness of the martensite [12, 13, 92, 93]. Most welding procedures for joining automotive steel sheets generally have low heat inputs causing fast cooling rates. Inasmuch as the lower critical cooling rate is due to higher alloying elements, the formation of martensite in welds is unavoidable. As a solution to this problem, several methods for changing the martensite formed in welds were proposed [9, 89]. By combining these trends, this chapter will explain the designs used for manufacturing medium Mn TRIP steel, the degradation of steel after welding, and solutions related to the formation of martensite with changes in the retained austenite.

4.1 Role of retained austenite in medium Mn TRIP steel weldment

The generic microstructural design strategy of the medium Mn TRIP steels is to have a stable retained austenite phase at room temperature, and hence many efforts have been made to obtain an optimal microstructure [90, 91, 94]. The production method varies depending on the purpose, but there are two major phase changes of the steel to be noted. The first is the martensitic transformation that occurs when the steel is heated above the Ac_3 temperature and subsequently cooled to room temperature (or a temperature between M_s and M_f temperature). This initial martensite is another major factors that determines the mechanical properties after subsequent heat treatment [91], and it is again dependent on whether the steel is made from hot-rolled or cold-rolled material. The subsequent heat treatment (called the intercritical annealing process) is the most important. This is because the martensite phase transforms into a dual-phase matrix of ferrite and austenite by the redistribution of alloying elements between the two phases. There are many factors that can affect the volume fraction and stability of the retained austenite, but the most important one is basically to give sufficient time and temperature for diffusion of substitutional manganese atoms [90].

Before explaining the change in retained austenite that occurs during welding, it is necessary to examine how the mechanical properties of the welds in the medium Mn TRIP steel appear. A considerable amount of manganese is used in this steel, resulting in higher carbon equivalent and a lower M_s temperature. The higher carbon equivalent generally lowers the cross-tension strength in AHSS resistance spot weldments. Oikawa et al. [95] reported that as the tensile strength of AHSS increases, the tensile-shear strength also increases while the cross-tension strength (CTS) decreases. In the resistance spot weldment (where the mechanical properties are mainly determined by the fracture mode of the weld), the high carbon equivalent causes crack propagation to the brittle HAZ or FZ rather than to the base metal or soft zone. This deterioration is also a problem in medium Mn TRIP steel regardless of the welding methods [12, 13, 93]. Figure 12 compares CTS and the button diameter of similar and dissimilar welded joints of medium Mn TRIP steel together with DP steel. The solid symbols in this graph represent the welded properties according to ISO18278-2, and the open symbols represent the properties after paint-baking heat treatment. The latter is discussed in the next section. Compared with conventional TRIP steel welds, the CTSs in similar and dissimilar welds of medium Mn TRIP steel are quite low. Both similar and dissimilar welds of conventional TRIP steel have CTS values more than 5 kN when welded at a 7.0 kA welding current. Figure 13 summarizes how failure modes appear in the similar and dissimilar resistance spot welds of medium Mn TRIP steel. Deterioration of the weld characteristics of the medium Mn steel was due to crack propagation to the center line of the FZ or to the CGHAZ. Of course, the spot weldment may show different failure modes depending on the size of the FZ, which is usually called the weld nugget size [96]. The overall trend in dissimilar welds, however, needs to be clarified as the crack propagates towards the CGHAZ [12].

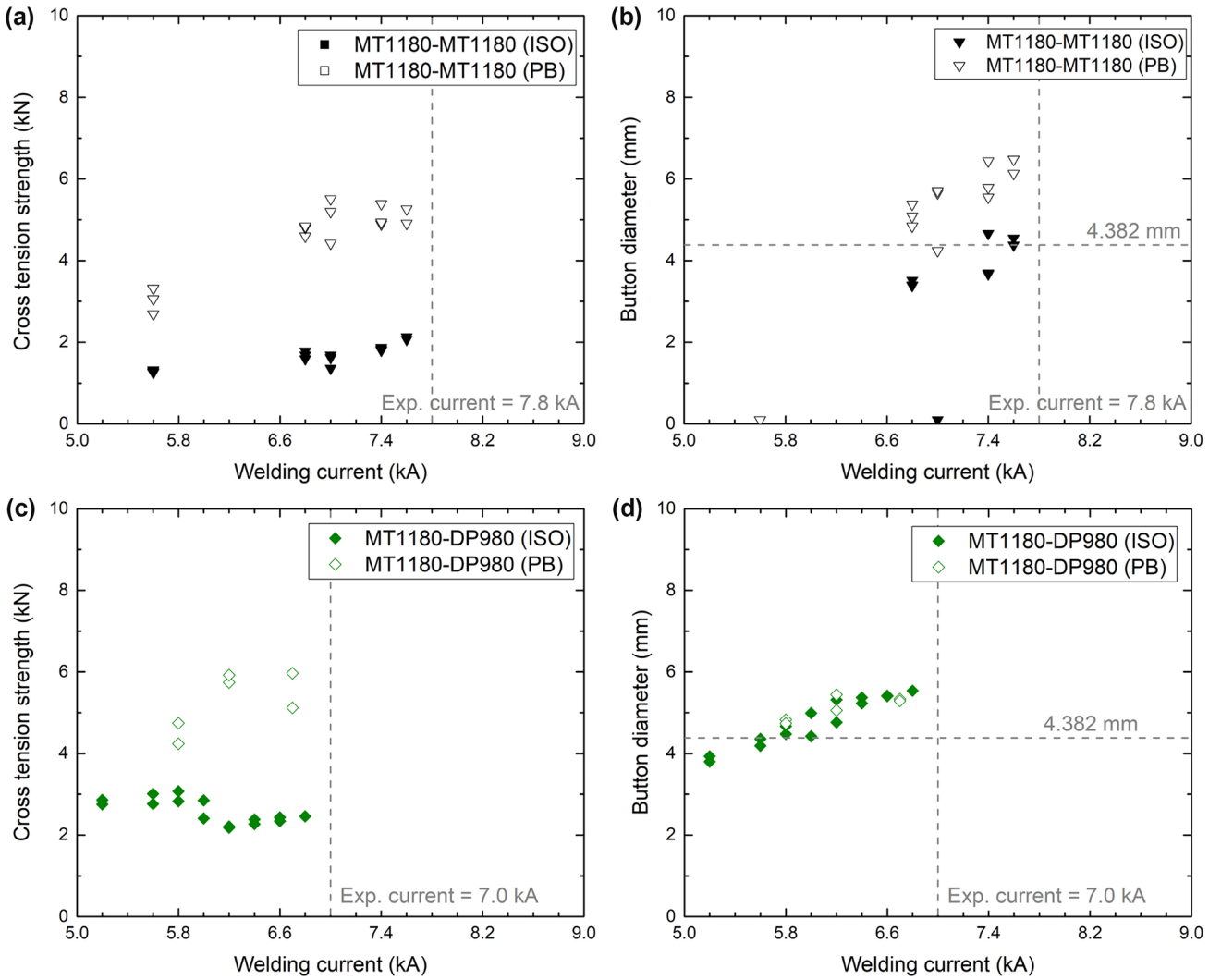

Fig. 12 Cross-tension test results for (**a**, **b**) similar MT1180/MT1180 and (**c**, **d**) dissimilar MT1180/DP980 welds. The solid symbols represent the properties in the as-welded state according to ISO18278-2, and the open symbols represent the properties after paint-baking heat treatment (Redrawn from [12, 92])

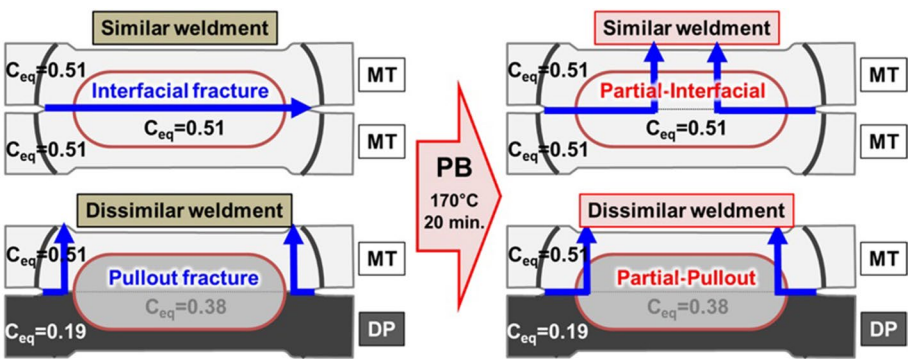

Fig. 13 Schematic illustrations of fracture mode changes for similar and dissimilar welds of medium Mn TRIP steel together with DP steel after paint-baking heat treatment (redrawn from [12, 92])

The retained austenite that is intentionally formed in the production stage of the steel will be transformed into martensite after welding. The manganese accumulated in this austenite will be uniformly distributed in the full austenite matrix to achieve thermodynamic equilibrium at the CGHAZ peak temperature, which is much higher than the

A_3 temperature. Therefore, the formation of martensite in the weld is inevitable considering both the very low critical cooling rate of the medium Mn TRIP steel and the fast cooling rate in the weldment. The martensite shows an extensive change in mechanical characteristics depending on the cooling rate under the critical cooling rate. Thus, the brittleness of martensite is related to insufficient self-tempering, as well as the improved CTS by paint-baking heat treatment which will be described below.

4.2 Improvement of cross-tension properties by paint-baking heat treatment

As already shown in Figs. 12 and 13, improved CTS after paint-baking heat treatment is related to changes in the fracture modes. The change in fracture behavior and hence improved mechanical properties in medium Mn TRIP steel welds implies that low temperature tempering at the CGHAZ is possible. The paint-baking heat treatment is one procedure in the automotive manufacturing process. This CGHAZ strengthening effect is equally applicable to the martensite produced during the steel stamping process [97]. As with other tempering mechanisms, it is naturally dominated by carbon diffusion because it is conducted at lower temperature. At temperatures below 170 °C, where the paint-baking is performed, only interstitial atoms have sufficient diffusion distances (within nanometers) along the lath or the boundaries. Carbide is formed under high heat treatment conditions, i.e., either higher temperature or longer time, and the mechanical properties are reduced again [92]. Therefore, designs considering low temperature tempering kinetics seems to be necessary. Ultimately, control of the alloying elements should be considered to solve the CGHAZ brittleness due to the decrease in retained austenite fraction.

5 Summary

In this review, the importance of research on the weldabilities of advanced Mn steels was highlighted with brief descriptions about the development history of recent advanced high strength steels for automotive applications. The principal features of the weldabilities of each steel are as follows:

1. High Mn TWIP steel has a considerable amount of alloying elements added to form single-phase austenite with an intermediate stacking fault energy at room temperature. The high manganese content of the steel lowers the weldability due to segregation along the dendritic boundary in the fusion zone. The hot cracking behavior of the steel is related to the solidification mode, and the addition of appropriate amounts of additional alloying element such as Al and Cr can improve solidification cracking susceptibility by forming primary delta ferrite. In the heat-affected zone, grain growth occurs without phase transformation and the degradation in the mechanical properties is not large.
2. In the high Mn lightweight steels, the effects of the welding process on the microstructural characteristics and mechanical properties are diverse because of the rapid phase transitions and deformation behavior. In the fusion zone, a complicated microstructural evolution occurs forming various ferrite, austenite, or DO3 phases induced by Al content, which results in ductility loss. Additional segregation or precipitation were also reported depending on the alloying elements (such as Cr). In the HAZ, the precipitation and dissolution behavior of intra-granular κ-carbide have significant effects on the tensile and hardness properties in the HAZ of lightweight steels, while inter-granular κ-carbide causes severe embrittlement. Based on these studies, delicate optimization of alloy and weld metal design is a key aspect to ensure stable properties and weldability in lightweight steels.
3. Medium Mn TRIP steels have a dual-phase matrix of ferrite and austenite containing intentionally redistributed manganese and carbon contents to obtain stable austenite at room temperature. However, regardless of similar and dissimilar weldment, coarse-grained HAZ and FZ undergo martensitic transformation during heating above the Ac_3 temperature and then rapid cooling to room temperature. Then the high retained austenite content is sharply reduced, resulting in deterioration of mechanical properties with increased brittleness. Various ways to improve weldability have been proposed, and the paint-baking heat treatment process during automotive production can drastically improve the tensile properties of martensite, even when conducted at low temperature.

Acknowledgements The authors thank the POSCO Technical Research Laboratory for their support.

References

1. *Passenger Car Miles Per Gallon (Normalized to CAFE)*www.theicct.org/chart-library-passenger-vehicle-fuel-economy. *Accessed 22 Mar 2020*
2. A.N. Kleit, Econ. Inq. **42**, 279–294 (2004)
3. J. Zielinski, R. Andreucci, N. Rajagopalan, C.B. Aktas, Resour. Conserv. Recycl. **136**, 466–472 (2018)
4. R. Kuziak, R. Kawalla, S. Waengler, Arch. Civ. Mech. Eng. **8**, 103–117 (2008)
5. D. Raabe, *Banana Diagram of Steel Properties* http://www.dierk-raabe.com/steels-brief-introduction/. Accessed 22 Mar 2020

6. D.-W. Suh, S.-J. Kim, Scr. Mater. **126**, 63–67 (2017)
7. L. Prém, Z. Bézi, A. Balogh, in *Vehicle and Automotive Engineering*, ed. by K. Jármai, B. Bolló (Springer, Berlin), pp. 407–423
8. L.T. Robertson, T.B. Hilditch, P.D. Hodgson, Int. J. Fatigue **30**, 587–594 (2008)
9. G. Park, G. Bae, C. Lee, Metall. Mater. Trans. A **50**, 1294–1307 (2019)
10. B.C. De Cooman, O. Kwon, K.G. Chin, Mater. Sci. Technol. **28**, 513–527 (2012)
11. J. Yoo, K. Han, Y. Park, J. Choi, C. Lee, Sci. Technol. Weld. Join. **19**, 514–520 (2014)
12. G. Park, K. Kim, S. Uhm, C. Lee, Mater. Sci. Eng. A **752**, 206–216 (2019)
13. Q. Jia, L. Liu, W. Guo, Y. Peng, G. Zou, Z. Tian, Y. Zhou, Metals **8**, 48 (2018)
14. M. Uchihara, Weld. Int. **25**, 249–259 (2011)
15. Y.S. Yang, S.H. Lee, J. Mater. Process. Technol. **94**, 151–156 (1999)
16. S. Daneshpour, S. Riekehr, M. Koçak, C.H.J. Gerritsen, Sci. Technol. Weld. Join. **14**, 20–25 (2009)
17. O. Bouaziz, S. Allain, C. Scott, Scr. Mater. **58**, 484–487 (2008)
18. J.W. Morris, *Iron-Manganese Steels for Cryogenic Use* (International Society of Offshore and Polar Engineers, Anchorage, 2013)
19. M. Choi, J. Lee, H. Nam, N. Kang, M. Kim, D. Cho, Met. Mater. Int. **26**, 240–247 (2020)
20. J. Yoo, K. Han, Y. Park, C. Lee, Mater. Chem. Phys. **148**, 499–502 (2014)
21. H. Lee, M.C. Jo, S.S. Sohn, S.-H. Kim, T. Song, S.-K. Kim, H.S. Kim, N.J. Kim, S. Lee, Mater. Charact. **147**, 233–241 (2019)
22. H. Vahiddastjerdi, A. Rezaeian, M.R. Toroghinejad, G. Dini, E. Ghassemali, Opt. Laser Technol. **120**, 105721 (2019)
23. V. Torganchuk, I. Vysotskiy, S. Malopheyev, S. Mironov, R. Kaibyshev, Mater. Sci. Eng. A **746**, 248–258 (2019)
24. G. Park, B. Kim, Y. Kang, H. Kang, C. Lee, Mater. Charact. **118**, 14–21 (2016)
25. G. Park, S. Jeong, H. Kang, C. Lee, Mater. Charact. **139**, 293–302 (2018)
26. D.-Y. Choi, A. Sharma, S.-H. Uhm, J.P. Jung, Met. Mater. Int. **25**, 219–228 (2019)
27. S. Kou, *Welding Metallurgy 2/E*, ISBN 0-471-43491-4 (Wiley, New York, 2003), pp. 431–446
28. J.C. Lippold, D.J. Kotecki, *Welding Metallurgy and Weldability of Stainless Steels*, Vol. 376. ISBN 0-471-47379-0 (Wiley, New York, 2005), p. 376
29. J. Lippold, W. Savage, Weld. J. **61**, 388 (1982)
30. Y. Arata, F. Matsuda, S. Saruwatari, Trans. JWRI **3**, 79–88 (1974)
31. J.A. Brooks, A.W. Thompson, Int. Mater. Rev. **36**, 16–44 (1991)
32. C. Lee, J. Yoo, Y. Park, J. Choi, *The Twenty-Third International Offshore and Polar Engineering Conference* (International Society of Offshore and Polar Engineers)
33. J. Yoo, B. Kim, Y. Park, C. Lee, J. Mater. Sci. **50**, 279–286 (2015)
34. J. Yoo, B. Kim, Y. Jeong, Y. Park, C. Lee, ISIJ Int. **55**, 257–263 (2015)
35. L. Mújica Roncery, S. Weber, W. Theisen, Scr. Mater. **66**, 997–1001 (2012)
36. I. Mejía, H. Hernández-Belmontes, C. Maldonado, MRS Adv. **2**, 3899–3908 (2018)
37. P. Lee, C. Chiu, Y. Gau, J. Wu, High Temp. Mater. Process. Lond. **10**, 141–144 (1992)
38. A. Hamada, L. Karjalainen, Can. Metall. Q. **45**, 41–48 (2006)
39. H.-H. Huang, T.-H. Chuang, Mater. Sci. Eng. A **292**, 90–95 (2000)
40. P.-C. Chen, C.-G. Chao, T.-F. Liu, Scr. Mater. **68**, 380–383 (2013)
41. R. You, P.-W. Kao, D. Gan, Mater. Sci. Eng. A **117**, 141–148 (1989)
42. C.-H. Seo, K.H. Kwon, K. Choi, K.-H. Kim, J. Kwak, S. Lee, N.J. Kim, Scr. Mater. **66**, 519–522 (2012)
43. D.-W. Suh, N.J. Kim, Scr. Mater **68**, 337–338 (2013)
44. W.K. Choo, J. Kim, J. Yoon, Acta Mater. **45**, 4877–4885 (1997)
45. J.S. Ku, N.J. Ho, S.C. Tjong, J. Mater. Sci. **28**, 2808–2814 (1993)
46. Z.-Y. Huang, A.-L. Hou, Y.-S. Jiang, P. Wang, Q. Shi, Q.-Y. Hou, X.-H. Liu, J. Iron. Steel Res. Int. **24**, 1190–1198 (2017)
47. S.-H. Kim, H. Kim, N.J. Kim, Nature **518**, 77–79 (2015)
48. H. Kim, D.-W. Suh, N.J. Kim, Sci. Technol. Adv. Mater. **14**, 014205 (2013)
49. S.-W. Park, J.Y. Park, K.M. Cho, J.H. Jang, S.-J. Park, J. Moon, T.-H. Lee, J.-H. Shin, Met. Mater. Int. **25**, 683–696 (2019)
50. C. Chu, H. Huang, P. Kao, D. Gan, Scr. Metall. Mater. **30**, 505–508 (1994)
51. W. Yang, C. Wan, J. Mater. Sci. **25**, 1821–1823 (1990)
52. G. Frommeyer, U. Brüx, Steel Res. Int. **77**, 627–633 (2006)
53. J.D. Yoo, K.-T. Park, Mater. Sci. Eng. A **496**, 417–424 (2008)
54. X.-F. Zhang, Y. Hao, L. De-Ping, L. Zhang, Z.-Y. Huang, C. Guang, Int. J. Iron Steel Res. **23**, 963–972 (2016)
55. K.-T. Park, G. Kim, S.K. Kim, S.W. Lee, S.W. Hwang, C.S. Lee, Met. Mater. Int. **16**, 1–6 (2010)
56. O. Acselrad, R. Simao, L. Pereira, C. Achete, I. Kalashnikov, E. Silva, Metall. Mater. Trans. A **33**, 3569–3573 (2002)
57. O. Acselrad, I. Kalashnikov, E. Silva, M.S. Khadyev, R. Simao, Met. Sci. Heat Treat. **48**, 543–553 (2006)
58. R.A. Howell, D.C. Van Aken, *Iron and Steel Technology* (2009)
59. S. Chen, R. Rana, A. Haldar, R.K. Ray, Prog. Mater Sci. **89**, 345–391 (2017)
60. K. Lee, S.-J. Park, J. Moon, J.-Y. Kang, T.-H. Lee, H.N. Han, Scr. Mater. **124**, 193–197 (2016)
61. K.-G. Chin, H.-J. Lee, J.-H. Kwak, J.-Y. Kang, B.-J. Lee, J. Alloys Compd. **505**, 217–223 (2010)
62. D. Connétable, P. Maugis, Intermetallics **16**, 345–352 (2008)
63. M.-S. Kim, Y.-B. Kang, C. Zhang, Y. Peng, P. Zhou, W. Zhang, Y. Du, D. Sergeev, E. Yazhenskikh, D. Kobertz, Calphad **51**, 1–416 (2015)
64. A. Bentley, J. Mater. Sci. Lett. **5**, 907–908 (1986)
65. J. Moon, S.-J. Park, C. Lee, H.N. Han, T.-H. Lee, C.-H. Lee, Metall. Mater. Trans. A **48**, 4500–4510 (2017)
66. K. Sato, K. Tagawa, Y. Inoue, Scr. Metall. **22**, 899–902 (1988)
67. M. Li, H. Chang, P. Kao, D. Gan, Mater. Chem. Phys. **59**, 96–99 (1999)
68. W. Song, W. Zhang, J. von Appen, R. Dronskowski, W. Bleck, *Steel Research International* (2015)
69. J. Lee, S. Park, H. Kim, S.-J. Park, K. Lee, M.-Y. Kim, P. P. Madakashira, H.N. Han, *Metals and Materials International* (2018), pp. 1–9
70. Y. Sutou, N. Kamiya, R. Umino, I. Ohnuma, K. Ishida, ISIJ Int. **50**, 893–899 (2010)
71. S. Chang, Y. Hsiau, M. Jahn, J. Mater. Sci. **24**, 1117–1120 (1989)
72. I. Kalashnikov, B. Ermakov, O. Aksel'rad, L. Pereira, Met. Sci. Heat Treat. **43**, 493–496 (2001)
73. C. Kim, S. Kwon, B. Lee, J. Moon, S. Park, J. Lee, H. Hong, Mater. Sci. Eng. A **673**, 108–113 (2016)
74. J. Moon, S.-J. Park, J.H. Jang, T.-H. Lee, C.-H. Lee, H.-U. Hong, D.-W. Suh, S.H. Kim, H.N. Han, B.H. Lee, Scr. Mater. **127**, 97–101 (2017)
75. J. Moon, H.-Y. Ha, S.-J. Park, T.-H. Lee, J.H. Jang, C.-H. Lee, H.N. Han, H.-U. Hong, J. Alloys Compd. **775**, 1136–1146 (2018)
76. G. Mills, LATERAL **550**, 3 (1977)
77. C.-P. Chou, C.-H. Lee, Metallography **23**, 231–240 (1989)
78. C.H. Chao, N.J. Ho, J. Mater. Sci. **27**, 4139–4144 (1992)
79. C.-P. Chou, C.-H. Lee, J. Mater. Sci. **25**, 1491–1496 (1990)
80. C.-P. Chou, C.-H. Lee, Metall. Trans. A **20**, 2559–2561 (1989)
81. C.-P. Chou, C.-H. Lee, Mater. Sci. Eng. A **118**, 137–146 (1989)
82. B. Kim, S. Jeong, S.-J. Park, J. Moon, C. Lee, Met. Mater. Int. **25**, 1019–1026 (2019)
83. Y. Lin, C. Chou, Scr. Metall. Mater. **27**, 67–70 (1992)

84. S. Tjong, S. Zhu, N. Ho, J. Ku, Mater. Sci. Technol. **13**, 251–256 (1997)
85. S. Jeong, B. Kim, J. Moon, S.-J. Park, C. Lee, Mater. Sci. Eng. A **726**, 223–230 (2018)
86. S. Jeong, G. Park, B. Kim, J. Moon, S.-J. Park, C. Lee, Mater. Sci. Eng. A (2018)
87. B. Kim, S. Jeong, S.-J. Park, J. Moon, C. Lee, Mater. Chem. Phys. **238**, 121904 (2019)
88. J. Moon, S.-J. Park, J. Weld. Join. **35**, 9–15 (2017)
89. X. Li, Y. Chang, C. Wang, P. Hu, H. Dong, Mater. Sci. Eng. A **679**, 240–248 (2017)
90. S. Lee, B.C. De Cooman, Metall. Mater. Trans. A **44**, 5018–5024 (2013)
91. J. Han, S.-J. Lee, J.-G. Jung, Y.-K. Lee, Acta Mater. **78**, 369–377 (2014)
92. G. Park, K. Kim, S. Uhm, C. Lee, Mater. Sci. Eng. A **766**, 138401 (2019)
93. N. Lun, D.C. Saha, A. Macwan, H. Pan, L. Wang, F. Goodwin, Y. Zhou, Mater. Des. **131**, 450–459 (2017)
94. J. Han, Y.-K. Lee, Acta Mater. **67**, 354–361 (2014)
95. H. Oikawa, G. Murayama, T. Sakiyama, Y. Takahashi, T. Ishikawa, Shinnittetsu Giho **385**, 36 (2006)
96. M. Pouranvari, S. Marashi, Sci. Technol. Weld. Join. **18**, 361–403 (2013)
97. Z.R. Hou, T. Opitz, X.C. Xiong, X.M. Zhao, H.L. Yi, Scr. Mater. **162**, 492–496 (2019)